ACS APPLIED ENERGY MATERIALS

www.acsaem.org Article

Molecularly Engineered Self-Assembled Monolayers as Effective Hole-Selective Layers for Organic Solar Cells

Mingliang Li,◆ Zhenzhu Li,◆ Huiting Fu,◆ Runze Yu,◆ Wenlin Jiang, Feng Qi, Francis R. Lin, Gang Chen,* Aron Walsh,* and Alex K.-Y. Jen*

Cite This: *ACS Appl. Energy Mater.* 2024, 7, 1306−1312 Read Online

ACCESS | Metrics & More | Article Recommendations | Supporting Information

ABSTRACT: Self-assembled monolayers (SAMs) are an emerging class of hole-selective layers (HSLs) to replace the conventional poly(3,4-ethylenedioxythiophene) polystyrenesulfonate (PEDOT:PSS) in organic solar cells (OSCs). Despite the wide use of SAMs, it is difficult to directly establish a feedback loop between material design and OSC performance as the SAM quality will also affect the OSC performance and was frequently neglected. In this work, we designed a series of carbazole-derived SAMs by engineering the halogen substituents and the alkyl linker lengths. A SAM stacking model was established to evaluate the SAM qualities in terms of surface morphology, molecular bonding, and packing quality. Consequently, the iodinated carbazole SAM with C2 spacer (Cz-I-2) showed the highest molecular regularity, the top OSC performance in the PM6:Y6 system, and good universal applicability with a power conversion efficiency (PCE) of 18.1% in the D18:Y6 system. It can be concluded that SAMs should benefit from OSC performance by achieving suitable energy level alignment, high packing regularity, and enhanced interactions with adjacent layers. Our work provides insight into designing SAMs for effective HSLs in efficient OSCs.

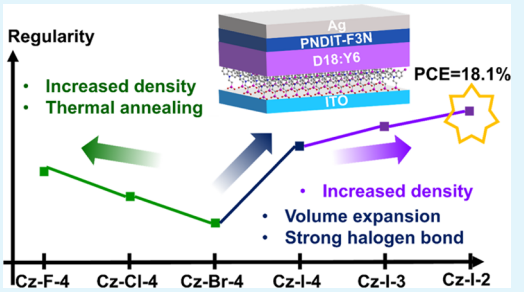

KEYWORDS: *self-assembled monolayers (SAMs), molecular engineering, stacking model, hole-selective layer (HSL), organic solar cells (OSCs)*

INTRODUCTION

Organic solar cells (OSCs) have received great attention as an important field in photovoltaic studies due to their potential advantages of high efficiency, outstanding flexibility, facile processability, and lightweight.[1−4] Currently, a basic OSC mainly consists of an anode, cathode, active layer, and charge-selective layers (CSLs) between the interfaces; therefore, good charge extraction and transport can be realized to benefit the device performance.[5−7] Among different CSLs for OSCs, the electron-selective layers (ESLs) have been extensively developed, where a wide variety of *n*-type materials such as ZnO, PFN-Br, and PNDIT-F3N, are commercially available.[8−10] In sharp contrast, as one of the few available options, PEDOT:PSS has been one of the very few solution-processable p-type materials used as the hole-selective layer (HSL) in OSCs. However, there are certain drawbacks to this material, such as corrosivity, hygroscopicity, high cost, and parasitic absorption. These limit the performance of OSCs and compromise the long-term stability of devices.[11,12] Therefore, it is urgent to develop new HSLs to further improve the performance of OSCs.

Recently, self-assembled monolayers (SAMs) offering high processability, low cost, and minimum material consumption have shown great capability in tuning the work function of the substrate and enhancing the stability of the device when applied as HSLs in OSCs. Simultaneously, it can be structurally modified to establish appropriate interactions with the adjacent layers in the device stack, ensuring carrier extraction and transport.[13−16] The majority of SAMs that have been applied in OSCs are based on carbazole scaffolds. Anthopoulos et al. obtained a maximum power conversion efficiency (PCE) of 18.03% with carbazole-based phosphonic acid SAM as the HSL in the PM6:BTP-eC9:$PC_{71}BM$ bulk-heterojunction (BHJ) cell.[17] Janssen et al. designed carbazole-based SAMs with different alkyl chains; thus, a high PCE of 17.4% was realized in the OSC based on PM6:BTP-eC9 with the C3-spacer SAM.[11] More recently, Hong et al. designed SAMs derived with a series of heteroatoms, which are universally effective for both perovskite solar cells and OSCs.[18]

Anthopoulos et al. explored halogen-substituted SAMs as HSLs and achieved a top PCE of 18.9% in doped PM6:PM7-Si:BTP-eC9 BHJs with chlorinated C2-spacer SAM.[19] Though pioneers have devoted themselves to molecular engineering of

Received: November 23, 2023
Revised: December 29, 2023
Accepted: December 29, 2023
Published: January 12, 2024

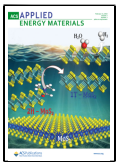

https://doi.org/10.1021/acsaem.3c02946
ACS Appl. Energy Mater. 2024, 7, 1306−1312

SAMs applied in photovoltaic devices,[11,18−20] so far, the SAM quality (particular packing regularity) has been rarely discussed in reported works on OSCs. This renders it difficult for other researchers in the field to understand the relationship among molecular structure, SAM stacking, and device performance, let alone establish a feedback loop to improve their material design rationales. To address this issue, herein we designed a series of SAM molecules Cz-I-2, Cz-I-3, and Cz-X-4 (X = F, Cl, Br, and I; Figure 1) taking advantages of both halogen-substituent and alkyl linker engineering and prepared design SAMs by spin coating to investigate their qualities on the indium tin oxide (ITO) substrate. On this basis, an assembly model of SAMs was established to correlate molecular design and SAM quality. In the device characterization with resulting SAMs, we found that OSCs based on Cz-I-2 SAMs with high regularity showed better performance and good universality, working with another active material system D18:Y6, whose PCE can reach more than 18%. The optimized device performance could be attributed to molecular energy level alignment, regular packing, and enhanced interaction with the adjacent layers. Our work provides practical experience in new material development and SAM quality control for effective HSLs and fabricating high-performance OSCs.

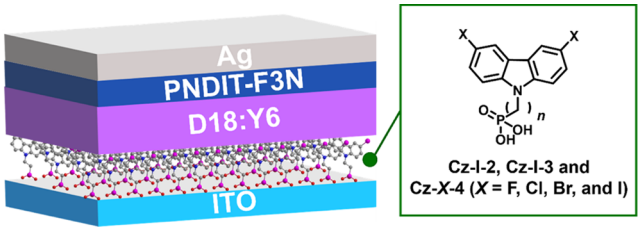

Figure 1. Schematic cross section of an OSC with designed SAMs as HSLs. The inset is the chemical structure of Cz-I-2, Cz-I-3, and Cz-X-4 (X = F, Cl, Br, and I). The numbers in the molecular names (*n*) are the linker lengths.

RESULTS AND DISCUSSION

The SAMs were designed with the conventional carbazole scaffold and phosphonic acid anchor group. Molecular engineering of the halogen substituents and alkyl linker lengths can synergistically modulate the SAM packing quality. The halogen substituents were grafted to modify the molecular energy level and adjust intramolecular and intermolecular interactions.[21,22] The variant alkyl linkers can directly modulate the material flexibility and the interaction between

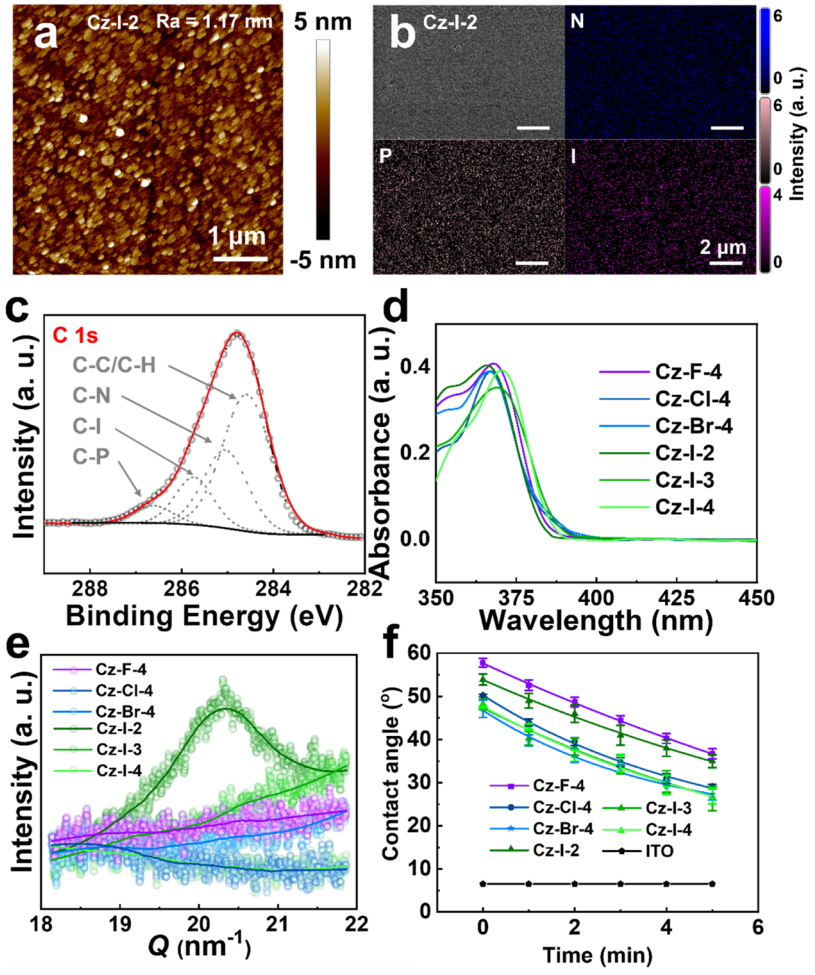

Figure 2. Characterization of SAMs. (a) AFM image of Cz-I-2 SAMs on ITO. (b) SEM and its corresponding N (blue), P (pink), and I (purple) EDS mappings of Cz-I-2 SAMs on ITO. (c) High-resolution XPS plots of C 1s of Cz-I-2 SAMs. (d) UV−vis spectra of designed SAMs on ITO. (e) GIXD mappings of SAMs. (f) Time-dependent contact angle tests of SAMs.

https://doi.org/10.1021/acsaem.3c02946
ACS Appl. Energy Mater. 2024, 7, 1306−1312

the other components.[23−25] The SAM-modified ITO substrates were fabricated by spin coating a 2 mM methanol solution of SAMs on plasma-cleaned ITO, followed by 80 °C annealing for 10 min and additional solvent cleaning. To evaluate the SAMs' quality, their features in terms of surface morphology, molecular bonding, and packing quality were systematically characterized.

The microstructure was investigated with atomic force microscopy (AFM) and scanning electron microscopy (SEM) techniques. In the AFM image (Figure 2a), the roughness (1.17 nm) for the Cz-I-2-modified substrate is comparable to that of bare ITO (1.02 nm), as the surface textures of substrate before and after ultrathin SAM modification were kept almost identical (Figure S1).[26] No severe aggregations at large scales of Cz-I-2 were detected as its characteristic elements (N, P, and I) were uniformly distributed on the substrate in the energy-dispersive spectroscopy (EDS, Figures 2b and S2).[27] We employed X-ray photoelectron spectroscopy (XPS) for the characterization of SAMs on solid surfaces, benefiting from its high sensitivity.[28,29] The C signals could be deconvoluted into 4 subpeaks by fitting, assigned to C−C/C-H, C−N, C−P, and C−I, respectively, and the O signals were fitted into 3 subpeaks, assigned to In−O−In, In−OH, and In−O−P/P═O (Figures 2c, S6, and S7).[17,30,31] The subpeaks not only demonstrate the formation of surface bonding but also provide detailed information on the different chemical nature of these bonds. As evidenced by the intensity trend of characteristic peaks in attenuated total reflection-Fourier transform infrared spectroscopy measurements (ATR-FTIR, Figure S8), it was demonstrated that as the halogen atomic number increases, the molecular concentration of the SAM decreases. On the other hand, shorter alkyl chains resulted in higher concentrations among the iodinated SAM molecules. The exact SAM coverages (Γ) were revealed by ultraviolet−visible spectroscopy-based method (UV−vis, Figures 2d and S9) in Table 1,[19] which was corroborated with trends in the ATR-FTIR analysis.

Table 1. SAM Coverage Calculated from UV−Vis Measurement[a]

SAM	$\varepsilon(\lambda)$ ($\times 10^4$ M cm^{-1})	Γ ($\times 10^{-9}$ mol cm^{-2})
Cz-F-4	4.30	9.51
Cz-Cl-4	3.71	8.70
Cz-Br-4	3.82	8.41
Cz-I-2	4.12	6.82
Cz-I-3	4.15	6.53
Cz-I-4	4.15	6.22

[a] $\varepsilon(\lambda)$ is the molar extinction coefficient of the SAM solution calculated from the absorbance maxima at ca. 380 nm.

A semiquantitative analysis by XPS was performed to reveal the regularity of SAMs (Table 2). Since a highly regular layer can shield the photoelectron from the bottom layer and attenuate the XPS signal, the difference coefficient between the atomic-sensitivity-factor-weighted C/P element ratio and the stoichiometric one (R_{ASF}/R_{number}), defined in eq S2, is selected as an indicator of the molecular regularity in SAMs. Therefore, iodinated carbazoles with high R_{ASF}/R_{number} values were found to have higher regularity, and the regularity could be further improved by reducing the alkyl chain length, giving Cz-I-2 the most ordered SAM. The top regularity of Cz-I-2 was further validated by GIXD with a diffraction peak at q = 2.03 Å^{-1} (Figure 2e) and contact angle measurements as the initial contact angle and the decay constant of exponential fitting (Figure 2f and Table S2) increased.[32] Moreover, in the ATR-FTIR (Figure S8), the shifts of two vibrations of the C−H stretch (a symmetric stretch at ca. 2851 cm^{-1} and an asymmetric stretch at ca. 2920 cm^{-1}) to the higher field indicate a disordered monolayer with cis C−C bonds, which show the same regularity trend in alkyl linkers.[33,34] Therefore, in this system of 3,6-dihalogenated carbazoles, shrinking the size of the halogens and shortening the alkyl chains in iodinated SAMs could improve the regularity. Based on the above results, we established a SAM assembly model to explain the relationship between the molecular structure and SAM stacking.

On this basis, an assembly model for SAMs based on 3,6-dihalogenated carbazoles is proposed in Figure 3a. The packing of the SAMs except for iodine-based ones is gradually optimized as the size of halogen shrinks. This can be explained as the Cz-F-4 and Cz-Cl-4 can be optimized in molecular packing when they are annealed above their glass-transition temperature (T_g, Figure S11), referring to the DSC measurements. On the other hand, increased densities synergistically optimize molecular packing owing to the stronger intermolecular interactions. The density functional theory (DFT) calculation in Figure 3b and Table S3 shows that the binding energies of SAM and the substrate increase as the halogen atoms shrink, demonstrating that it is easier for Cz-F-4 and Cz-Cl-4 to bind to the substrate to form a dense and regular packing. Unexpectedly, Cz-I-4 shows an unusual trend of a high regularity with strong rigidity, even at low concentrations, which may be attributed to the iodine's big atomic radius (Table S4) and the strong halogen bonds.[35,36] The large atomic radius can modulate the intermolecular distance and directly enhance the molecular interactions together with halogen bonds to reach a higher regularity. As shown in Figure 3a, the strengthened interactions can even keep iodinated carbazoles standing up straight to achieve a high regularity in the molecular dynamics (MD) simulations. To support the hypothesis, we further carried out MD simulations on systems with different molecular concentrations and calculated the distribution of regularity with parameter θ, where θ is the angle between the molecule and the substrate (Figure 3c). A low standard deviation of θ indicates concentrated conformations and high regularity, which results from strong intermolecular interactions. On such a basis, the standard deviation of θ for Cz-Br-4 at the high concentration was found to be bigger than that of Cz-I-4 even at low concentrations, demonstrating the high regularities of iodinated carbazole SAMs (Figure 3d). In terms of different alkyl linkers, the short chain in Cz-I-2 leads to small volumes, which is beneficial to its higher densities, stronger interactions, and thus higher regularity. The halogens and alkyl chains in halogenated carbazole SAMs work synergistically to regulate the flexibility and molecular size, as well as further differentiate the SAM density and intermolecular interactions, resulting in the diversity in molecular packing.

The application of designed SAMs was explored and compared to the PEDOT:PSS as HSLs in OSCs with a device configuration of ITO/HSL/PM6:Y6/PNDIT-F3N/Ag (Table 3 and Figure 4). Figure 4a shows the representative current density versus voltage (J−V) curves, and Table 3 summarizes the related photovoltaic parameters of derived OSCs. The designed SAMs exhibited a significant difference in terms of their OSC performances. In the comparison of Cz-X-4 (X = F,

https://doi.org/10.1021/acsaem.3c02946
ACS Appl. Energy Mater. 2024, 7, 1306−1312

Table 2. Atomic Concentration Summary of SAMs from XPS Analysis[a]

	atomic concentration (%)									
	C 1s	O 1s	N 1s	P 2p	X	In 3d	$R_{intensity}$	R_{ASF}	R_{number}	R_{ASF}/R_{number}
blank	13.04	16.13				62.29				
Cz-F-4	16.42	18.13	2.07	1.12	8.34 (F 1s)	45.58	14.66	22.87	16	1.43
Cz-Cl-4	14.61	21.42	2.33	1.00	6.79 (CI 2p)	48.23	14.61	22.79	16	1.42
Cz-Br-4	14.94	20.68	1.78	1.04	5.17 (Br 3d)	50.56	14.37	22.42	16	1.40
Cz-I-2	12.36	11.25	1.38	0.75	19.24(I 3d)	50.94	16.48	25.71	14	1.84
Cz-I-3	11.85	11.36	1.23	0.72	19.10(1 3d)	50.62	16.46	25.68	15	1.71
Cz-I-4	11.23	14.47	1.16	0.69	15.78 (I 3d)	50.42	16.28	25.40	16	1.59

[a] R_{ASF}, R_{number}, and $R_{intensity}$ are the atomic-sensitivity-factor-weighted element ratio, stoichiometric ratio, and XPS intensity ratio of C/P, respectively.

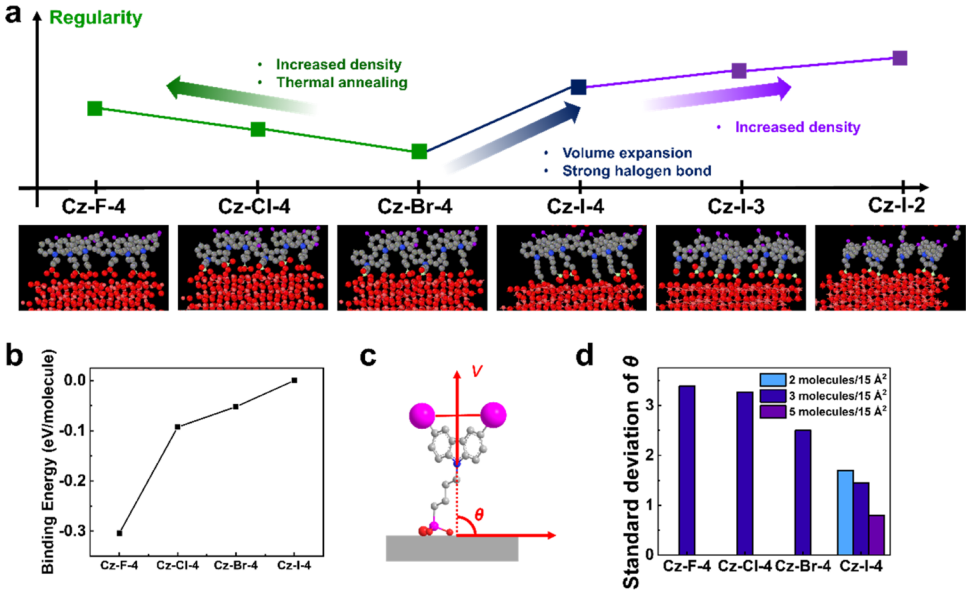

Figure 3. (a) Assembly trends and SAM regularities for designed SAMs. The images for MD calculations of 3 molecules in the 15 Å^2 area of ITO are shown below. (b) Binding energies from Table S3. The binding energy of Cz-I-4 is set as 0 for reference. (c) Definition of θ to indicate the changing of molecular configurations. The vector from nitrogen to the midpoint of the line connecting the halogen atoms is v, and the angle between v and the substrate is θ. (d) The standard deviations of θ for SAMs under different concentrations.

Table 3. OSC Performances with SAMs as HSLs in the PM6:Y6 System

HSLs	V_{oc} (V)	J_{sc} (mA/cm^2)	J_{cal} (mA/cm^2)	FF (%)	PCE (%)
PEDOT:PSS	0.861	26.0	25.5	74.3	16.6
Cz-Br-2	0.859	26.6		72.5	16.5
Cz-F-4	0.847	26.5	25.9	61.7	13.8
Cz-Cl-4	0.853	26.7	26.0	63.0	14.3
Cz-Br-4	0.856	26.6	25.9	67.6	15.4
Cz-I-2	0.865	26.9	26.2	75.8	17.6
Cz-I-3	0.863	26.8	26.1	74.6	17.3
Cz-I-4	0.855	26.8	26.1	70.0	16.0

Cl, Br, and I), the resulting device performances gradually enhanced as the size of halogen expanded, which can be attributed to the energy alignment (Figure S13). The Fermi levels of the electrodes can be simultaneously modulated by molecular density and an effective dipole perpendicular to the substrate. The ones based on iodinated SAM show well-matching energy levels with PM6, and the PCE of the Cz-I-4 device was dramatically enhanced to 16.0%, with a fill factor (FF) of 70.0%, a V_{oc} of 0.855 V, and a J_{sc} of 26.8 mA·cm^{-2} under 1 sun illumination (AM 1.5G, 100 mW·cm^{-2}). Furthermore, the device efficiency could be further improved with shorter alkyl linkers in iodinated SAMs owing to the deeper electrode Fermi level with higher molecular density and regularity. Consequently, Cz-I-2-based OSCs delivered a significantly increased PCE of 17.6%, with a largely improved FF of 75.8%, a V_{oc} of 0.865 V, and a J_{sc} of 26.9 mA·cm^{-2}, much higher than the previously reported Cz-Br-2 devices with a PCE of 16.5%, an FF of 72.5%, a V_{oc} of 0.859 V, and a J_{sc} of 26.6 mA·cm^{-2}.[37] It should be noted that the changes in device performance were mainly caused by the distinct FF values, while the modifications on molecular structures showed a negligible impact on J_{sc} as supported by their similar external quantum efficiency (EQE) spectra (Figure 4b). The enhancement of FF could be attributed to the improved surface quality with the ordered assemblies and stronger interactions,[38] where I atoms could be exposed and effectively interact with heteroatoms in the active layers,[39,40] validated by consistent surface energy evidenced by contact angle measurements in Table S5.[41,42] On the other hand, a shorter alkyl chain can also reduce the carrier hopping barriers and enhance the OSC device performance. Cz-I-2 showed good universality with another active system consisting of D18:Y6, delivering a good PCE of 18.1% with an FF of 77.5%, a V_{oc} of 0.854 V, and a J_{sc}

https://doi.org/10.1021/acsaem.3c02946
ACS Appl. Energy Mater. 2024, 7, 1306−1312

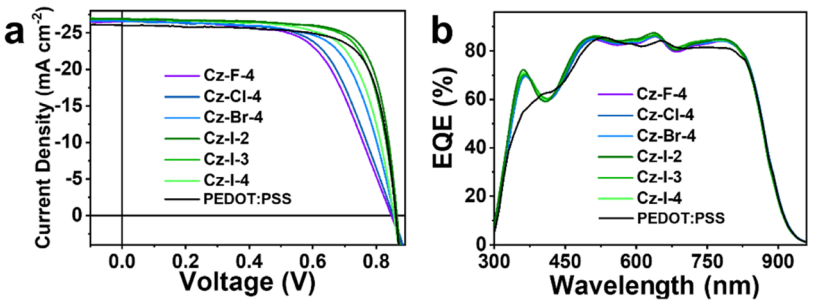

Figure 4. Performances of the OSC devices with designed SAMs as HSLs in the PM6:Y6 system. (a) J−V curves and (b) EQE curves.

of 27.3 mA·cm^{-2} (Figure S19). Interestingly, different trends in OSC performance were found in previous works.[11,19] Compared to our design, these molecular structures tailored by a single strategy (halogen substituents or alkyl linker lengths) may induce variations in intermolecular interactions and retention volumes during spin coating, which consequently will lead to disparities in the surface-adsorbed-SAM density and molecular conformation. These effects have a dual impact, influencing both ITO surface passivation and energy alignment via effective dipole toward the substrate. Moreover, different compositions of the organic semiconductors could exhibit variant affinity with SAMs, which further exacerbates the disparity in device performance. Therefore, factors including strong packing regularity, energy level alignment, and enhanced interaction with adjacent layers should be considered to design a SAM as an effective HSL in OSCs.

CONCLUSIONS

In conclusion, we modified and explored carbazole-based SAMs as effective HSLs in OSCs by engineering halogen substituents and alkyl linker chains. It was found that halogens worked in concert with alkyl chains to change the intramolecular interaction and SAM density to optimize the packing quality. On this basis, a SAM packing model was established for the relationship between the molecular structure and SAM regularity. Cz-I-2 SAMs showed the top OSC performance with the PM6:Y6 blend as the active layer, and its universality was proved with the D18:Y6 system to show a PCE of more than 18%. It can be concluded that SAMs should benefit OSC performance by achieving good energy level alignment, high packing regularity, and enhanced interaction with adjacent layers. This work provides experimental experience for the design and processing of SAMs working as effective HSLs, as well as applications in high-performance OSCs.

ASSOCIATED CONTENT

Supporting Information

The Supporting Information is available free of charge at https://pubs.acs.org/doi/10.1021/acsaem.3c02946.

Molecular synthesis; general methods for characterization and device fabrication; full names for the abbreviations; property table of halogen atoms and halogenated carbazoles; XPS survey of bare ITO as a reference; and orbital contributions to each energy level (PDF)

AUTHOR INFORMATION

Corresponding Authors

Gang Chen − *School of Physical Science and Technology, ShanghaiTech University, Shanghai 201210, China; Shanghai Synchrotron Radiation Facility, Shanghai Institute of Applied Physics, Chinese Academy of Sciences, Shanghai 201204, China;* orcid.org/0000-0001-8112-3579; Email: gchen@shanghaitech.edu.cn

Aron Walsh − *Department of Materials, Imperial College London, London SW7 2AZ, United Kingdom; Department of Physics, Ewha Womans University, Seoul 03760, Korea;* orcid.org/0000-0001-5460-7033; Email: a.walsh@imperial.ac.uk

Alex K.-Y. Jen − *Department of Materials Science and Engineering, City University of Hong Kong, Kowloon, Hong Kong 999077, China; Department of Chemistry, Hong Kong Institute for Clean Energy, and State Key Laboratory of Marine Pollution, City University of Hong Kong, Kowloon, Hong Kong 999077, China;* orcid.org/0000-0002-9219-7749; Email: alexjen@cityu.edu.hk

Authors

Mingliang Li − *Department of Materials Science and Engineering, City University of Hong Kong, Kowloon, Hong Kong 999077, China; Hong Kong Institute for Clean Energy and State Key Laboratory of Marine Pollution, City University of Hong Kong, Kowloon, Hong Kong 999077, China;* orcid.org/0000-0002-6181-5954

Zhenzhu Li − *Department of Materials, Imperial College London, London SW7 2AZ, United Kingdom; Department of Physics, Ewha Womans University, Seoul 03760, Korea;* orcid.org/0000-0002-6669-563X

Huiting Fu − *Department of Materials Science and Engineering, City University of Hong Kong, Kowloon, Hong Kong 999077, China; Hong Kong Institute for Clean Energy and State Key Laboratory of Marine Pollution, City University of Hong Kong, Kowloon, Hong Kong 999077, China*

Runze Yu − *School of Physical Science and Technology, ShanghaiTech University, Shanghai 201210, China; Shanghai Synchrotron Radiation Facility, Shanghai Institute of Applied Physics, Chinese Academy of Sciences, Shanghai 201204, China*

Wenlin Jiang − *Department of Materials Science and Engineering, City University of Hong Kong, Kowloon, Hong Kong 999077, China; Hong Kong Institute for Clean Energy and State Key Laboratory of Marine Pollution, City University of Hong Kong, Kowloon, Hong Kong 999077, China*

https://doi.org/10.1021/acsaem.3c02946
ACS Appl. Energy Mater. 2024, 7, 1306−1312

Feng Qi − *Department of Chemistry, Hong Kong Institute for Clean Energy, and State Key Laboratory of Marine Pollution, City University of Hong Kong, Kowloon, Hong Kong 999077, China;* orcid.org/0000-0003-3814-3317

Francis R. Lin − *Department of Chemistry, Hong Kong Institute for Clean Energy, and State Key Laboratory of Marine Pollution, City University of Hong Kong, Kowloon, Hong Kong 999077, China;* orcid.org/0000-0002-4651-9145

Complete contact information is available at: https://pubs.acs.org/10.1021/acsaem.3c02946

Author Contributions

◆M.L., Z.L., H.F., and R.Y. contributed equally to this work. Z.L. and A.W. performed the theoretical calculation. H.F. fabricated and tested the OSCs. R.Y. and G.C. conducted the GIXD tests. W.J. and F.Q. participated in the discussion. M.L. conducted the rest of the experiments. A.K.-Y.J., F.R.L., and M.L. raised this project and wrote the paper. The manuscript was written through contributions of all authors. All authors have given approval to the final version of the manuscript.

Funding

A.K.-Y.J. thanks the sponsorship of the Lee Shau-Kee Chair Professor (Materials Science) and the support from the APRC Grant of the City University of Hong Kong (9380086, 9610508), the TCFS Grant (GHP/018/20SZ) and MRP Grant (MRP/040/21X) from the Innovation and Technology Commission of Hong Kong, the Green Tech Fund (202020164) from the Environment and Ecology Bureau of Hong Kong, the GRF grants (11307621, 11316422) from the Research Grants Council of Hong Kong, Shenzhen Science and Technology Program (SGDX20201103095412040), the Guangdong Major Project of Basic and Applied Basic Research (2019B030302007), the Guangdong-Hong Kong-Macao Joint Laboratory of Optoelectronic and Magnetic Functional Materials (2019B121205002), the U.S. Office of Naval Research (N00014−20−1−2191), and the CRF grant (C6023−19GF) from the Research Grants Council of Hong Kong.

Notes

The authors declare no competing financial interest.

■ ABBREVIATIONS

SAMs, self-assembled monolayers; OSCs, organic solar cells; HSLs, hole-selective layers; PCE, power conversion efficiency; CSLs, charge-selective layers; ESLs, electron-selective layers; BHJ, bulk-heterojunction; ITO, indium tin oxide; XPS, X-ray photoelectron spectroscopy; GIXD, grazing incidence X-ray diffraction; AFM, atomic force microscope; SEM, scanning electron microscope; EDS, energy-dispersive spectroscopy; ATR-FTIR, attenuated total reflection-Fourier transform infrared spectroscopy; UV−vis, ultraviolet−visible spectroscopy; MD, molecular dynamics

■ REFERENCES

(1) Wu, X.; Li, B.; Zhu, Z.; Chueh, C.-C.; Jen, A. K.-Y. Designs from single junctions, heterojunctions to multijunctions for high-performance perovskite solar cells. *Chem. Soc. Rev.* **2021**, *50*, 13090−13128.

(2) Gao, W.; Jiang, M.; Wu, Z.; Fan, B.; Jiang, W.; Cai, N.; Xie, H.; Lin, F. R.; Luo, J.; An, Q.; Woo, H. Y.; Jen, A. K.-Y. Intramolecular chloro−sulfur interaction and asymmetric side-chain isomerization to balance crystallinity and miscibility in all-small-molecule solar cells. *Angew. Chem., Int. Ed.* **2022**, *61*, No. 202205168, DOI: 10.1002/anie.202205168.

(3) Qi, F.; Jiang, K.; Lin, F.; Wu, Z.; Zhang, H.; Gao, W.; Li, Y.; Cai, Z.; Woo, H. Y.; Zhu, Z.; Jen, A. K.-Y. Over 17% efficiency binary organic solar cells with photoresponses reaching 1000 nm enabled by selenophene-fused nonfullerene acceptors. *ACS Energy Lett.* **2021**, *6*, 9−15.

(4) Yao, H.; Ye, L.; Zhang, H.; Li, S.; Zhang, S.; Hou, J. Molecular design of benzodithiophene-based organic photovoltaic materials. *Chem. Rev.* **2016**, *116*, 7397−7457.

(5) Po, R.; Carbonera, C.; Bernardi, A.; Camaioni, N. The role of buffer layers in polymer solar cells. *Energy Environ. Sci.* **2011**, *4*, 285−310.

(6) Ma, H.; Yip, H.-L.; Huang, F.; Jen, A. K.-Y. Interface engineering for organic electronics. *Adv. Funct. Mater.* **2010**, *20*, 1371−1388.

(7) Yip, H.-L.; Jen, A. K.-Y. Recent advances in solution-processed interfacial materials for efficient and stable polymer solar cells. *Energy Environ. Sci.* **2012**, *5*, 5994−6011.

(8) Fu, H.; Li, Y.; Yu, J.; Wu, Z.; Fan, Q.; Lin, F.; Woo, H. Y.; Gao, F.; Zhu, Z.; Jen, A. K.-Y. High efficiency (15.8%) all-polymer solar cells enabled by a regioregular narrow bandgap polymer acceptor. *J. Am. Chem. Soc.* **2021**, *143*, 2665−2670.

(9) Zhang, G.; Lin, F. R.; Qi, F.; Heumüller, T.; Distler, A.; Egelhaaf, H.-J.; Li, N.; Chow, P. C. Y.; Brabec, C. J.; Jen, A. K. Y.; Yip, H.-L. Renewed prospects for organic photovoltaics. *Chem. Rev.* **2022**, *122*, 14180−14274, DOI: 10.1021/acs.chemrev.1c00955.

(10) Yip, H.-L.; Hau, S. K.; Baek, N. S.; Ma, H.; Jen, A. K.-Y. Polymer solar cells that use self-assembled-monolayer- modified ZnO/metals as cathodes. *Adv. Mater.* **2008**, *20*, 2376−2382.

(11) Bin, H.; Datta, K.; Wang, J.; van der Pol, T. P. A.; Li, J.; Wienk, M. M.; Janssen, R. A. J. Finetuning hole-extracting monolayers for efficient organic solar cells. *ACS Appl. Mater. Interfaces* **2022**, *14*, 16497−16504.

(12) Lin, Y.; Adilbekova, B.; Firdaus, Y.; Yengel, E.; Faber, H.; Sajjad, M.; Zheng, X.; Yarali, E.; Seitkhan, A.; Bakr, O. M.; El-Labban, A.; Schwingenschlögl, U.; Tung, V.; McCulloch, I.; Laquai, F.; Anthopoulos, T. D. 17% Efficient organic solar cells based on liquid exfoliated WS_2 as a replacement for PEDOT:PSS. *Adv. Mater.* **2019**, *31*, No. 1902965.

(13) Niu, T.; Xue, Q.; Yip, H.-L. Molecularly engineered interfaces in metal halide perovskite solar cells. *J. Phys. Chem. Lett.* **2021**, *12*, 4882−4901.

(14) Li, F.; Jen, A. K.-Y. Interface engineering in solution-processed thin-film solar cells. *Acc. Mater. Res.* **2022**, *3*, 272−282.

(15) Hau, S. K.; Yip, H.-L.; Ma, H.; Jen, A. K.-Y. High performance ambient processed inverted polymer solar cells through interfacial modification with a fullerene self-assembled monolayer. *Appl. Phys. Lett.* **2008**, *93*, No. 233304.

(16) Li, M.; Xie, Y.; Lin, F. R.; Li, Z.; Yang, S.; Jen, A. K.-Y. Self-assembled monolayers as emerging hole-selective layers enable high-performance thin-film solar cells. *Innovation* **2023**, *4*, No. 100369.

(17) Lin, Y.; Firdaus, Y.; Isikgor, F. H.; Nugraha, M. I.; Yengel, E.; Harrison, G. T.; Hallani, R.; El-Labban, A.; Faber, H.; Ma, C.; Zheng, X.; Subbiah, A.; Howells, C. T.; Bakr, O. M.; McCulloch, I.; Wolf, S. D.; Tsetseris, L.; Anthopoulos, T. D. Self-assembled monolayer enables hole transport layer-free organic solar cells with 18% efficiency and improved operational stability. *ACS Energy Lett.* **2020**, *5*, 2935−2944.

(18) Ullah, A.; Park, K. H.; Lee, Y.; Park, S.; Faheem, A. B.; Nguyen, H. D.; Siddique, Y.; Lee, K.-K.; Jo, Y.; Han, C.-H.; Ahn, S.; Jeong, I.; Cho, S.; Kim, B.; Park, Y. S.; Hong, S. Versatile Hole Selective Molecules Containing a Series of Heteroatoms as Self-Assembled Monolayers for Efficient p-i-n Perovskite and Organic Solar Cells. *Adv. Funct. Mater.* **2022**, *32*, No. 2208793.

(19) Lin, Y.; Zhang, Y.; Zhang, J.; Marcinskas, M.; Malinauskas, T.; Magomedov, A.; Nugraha, M. I.; Kaltsas, D.; Naphade, D. R.; Harrison, G. T.; El-Labban, A.; Barlow, S.; De Wolf, S.; Wang, E.; McCulloch, I.; Tsetseris, L.; Getautis, V.; Marder, S. R.; Anthopoulos, T. D. 18.9% Efficient organic solar cells based on n-doped bulk-

heterojunction and halogen-substituted self-assembled monolayers as hole extracting interlayers. *Adv. Energy Mater.* **2022**, *12*, No. 2202503.
(20) Al-Ashouri, A.; Köhnen, E.; Li, B.; Magomedov, A.; Hempel, H.; Caprioglio, P.; Márquez, J. A.; Vilches, A. B. M.; Kasparavicius, E.; Smith, J. A.; Phung, N.; Menzel, D.; Grischek, M.; Kegelmann, L.; Skroblin, D.; Gollwitzer, C.; Malinauskas, T.; Jošt, M.; Matič, G.; Rech, B.; Schlatmann, R.; Topič, M.; Korte, L.; Abate, A.; Stannowski, B.; Neher, D.; Stolterfoht, M.; Unold, T.; Getautis, V.; Albrecht, S. Monolithic perovskite/silicon tandem solar cell with > 29% efficiency by enhanced hole extraction. *Science* **2020**, *370*, 1300−1309, DOI: 10.1126/science.abd4016.
(21) Guo, Q.; Zhou, S.; Li, X.; Tao, L.; Li, M.; Su, S.-J.; Wan, D.; Li, J. Ultralong room-temperature phosphorescence remarkably weakened by halogenation-induced molecular packing in hexaphenylmelamine derivatives. *Chem. Commun.* **2021**, *57*, 6177−6180.
(22) Zou, Y.; Chen, H.; Bi, X.; Xu, X.; Wang, H.; Lin, M.; Ma, Z.; Zhang, M.; Li, C.; Wan, X.; Long, G.; Zhaoyang, Y.; Chen, Y. Peripheral halogenation engineering controls molecular stacking to enable highly efficient organic solar cells. *Energy Environ. Sci.* **2022**, *15*, 3519−3533.
(23) Acton, O.; Ting, G.; Ma, H.; Ka, J. W.; Yip, H.-L.; Tucker, N. M.; Jen, A. K.-Y. π-σ-Phosphonic acid organic monolayer/sol−gel hafnium oxide hybrid dielectrics for low-voltage organic transistors. *Adv. Mater.* **2008**, *20*, 3697−3701.
(24) Wang, G.; Li, M.; Wei, Q.; Xiong, Y.; Li, J.; Li, Z.; Tang, J.; Wei, F.; Tu, H. Design of an AIE-Active Flexible Self-Assembled Monolayer Probe for Trace Nitroaromatic Compound Explosive Detection. *ACS Sens.* **2021**, *6*, 1849−1856.
(25) Chen, H.; Li, M.; Lu, Z.; Wang, X.; Yang, J.; Wang, Z.; Zhang, F.; Gu, C.; Zhang, W.; Sun, Y.; Sun, J.; Zhu, W.; Guo, X. Multistep nucleation and growth mechanisms of organic crystals from amorphous solid states. *Nat. Commun.* **2019**, *10*, No. 3872.
(26) Hutchins, D. O.; Weidner, T.; Baio, J.; Polishak, B.; Acton, O.; Cernetic, N.; Ma, H.; Jen, A. K.-Y. Effects of self-assembled monolayer structural order, surface homogeneity and surface energy on pentacene morphology and thin film transistor device performance. *J. Mater. Chem. C* **2013**, *1*, 101−113.
(27) Jiang, W.; Li, F.; Li, M.; Qi, F.; Lin, F. R.; Jen, A. K.-Y. π-Expanded Carbazoles as Hole-Selective Self-Assembled Monolayers for High-Performance Perovskite Solar Cells. *Angew. Chem., Int. Ed.* **2022**, *61*, No. 202213560, DOI: 10.1002/anie.202213560.
(28) Chen, H.; Cheng, N.; Ma, W.; Li, M.; Hu, S.; Gu, L.; Meng, S.; Guo, X. Design of a photoactive hybrid bilayer dielectric for flexible nonvolatile organic memory transistors. *ACS Nano* **2016**, *10*, 436−445.
(29) Arndt, N. B.; Schlüter, F.; Böckmann, M.; Adolphs, T.; Arlinghaus, H. F.; Doltsinis, N. L.; Ravoo, B. J. Self-Assembled monolayers of arylazopyrazoles on glass and silicon oxide: Photoisomerization and photoresponsive wettability. *Langmuir* **2022**, *38*, 735−742.
(30) Deng, X.; Qi, F.; Li, F.; Wu, S.; Lin, F. R.; Zhang, Z.; Guan, Z.; Yang, Z.; Lee, C.-S.; Jen, A. K.-Y. Co-assembled monolayers as hole-selective contact for high-performance inverted perovskite solar cells with optimized recombination loss and long-term stability. *Angew. Chem., Int. Ed.* **2022**, *61*, No. 202203088.
(31) Ullah, A.; Park, K. H.; Nguyen, H. D.; Siddique, Y.; Shah, S. F. A.; Tran, H.; Park, S.; Lee, S. I.; Lee, K.-K.; Han, C.-H.; Kim, K.; Ahn, S.; Jeong, I.; Park, Y. S.; Hong, S. Novel phenothiazine-based self-assembled monolayer as a hole selective contact for highly efficient and stable p-i-n perovskite solar cells. *Adv. Energy Mater.* **2022**, *12*, No. 2103175.
(32) Liu, M.; Bi, L.; Jiang, W.; Zeng, Z.; Tsang, S.-W.; Lin, F. R.; Jen, A. K.-Y. Compact hole-selective self-assembled monolayers enabled by disassembling micelles in solution for efficient perovskite solar cells. *Adv. Mater.* **2023**, *35*, No. 2304415.
(33) Ting, G. G., II; Acton, O.; Ma, H.; Ka, J. W.; Jen, A. K.-Y. Study on the formation of self-assembled monolayers on sol−gel processed hafnium oxide as dielectric layers. *Langmuir* **2009**, *25* (4), 2140−2147.
(34) Snyder, R. G.; Strauss, H. L.; Elliger, C. A. Carbon-hydrogen stretching modes and the structure of n-alkyl chains. 1. Long, disordered chains. *J. Phys. Chem. A* **1982**, *86* (26), 5145−5150.
(35) Metrangolo, P.; Pilati, T.; Resnati, G. Halogen bonding and other noncovalent interactions involving halogens: a terminology issue. *CrystEngComm* **2006**, *8*, 946−947.
(36) Terraneo, G.; Resnati, G.; Metrangolo, P.*Iodine Chemistry and Applications*; Wiley, 2014; pp 159−194.
(37) Lin, Y.; Magomedov, A.; Firdaus, Y.; Kaltsas, D.; El-Labban, A.; Faber, H.; Naphade, D. R.; Yengel, E.; Zheng, X.; Yarali, E.; Chaturvedi, N.; Loganathan, K.; Gkeka, D.; AlShammari, S. H.; Bakr, O. M.; Laquai, F.; Tsetseris, L.; Getautis, V.; Anthopoulos, T. D. 18.4% Organic solar cells using a high ionization energy self-assembled monolayer as hole-extraction interlayer. *ChemSusChem* **2021**, *14*, 3569−3578.
(38) Jao, M.-H.; Liao, H.-C.; Su, W.-F. Achieving a high fill factor for organic solar cells. *J. Mater. Chem. A* **2016**, *4*, 5784−5801.
(39) Cai, G.; Chen, Z.; Xia, X.; Li, Y.; Wang, J.; Liu, H.; Sun, P.; Li, C.; Ma, R.; Zhou, Y.; Chi, W.; Zhang, J.; Zhu, H.; Xu, J.; Yan, H.; Zhan, X.; Lu, X. Pushing the Efficiency of High Open-Circuit Voltage Binary Organic Solar Cells by Vertical Morphology Tuning. *Adv. Sci.* **2022**, *9*, No. 2200578.
(40) Lommerse, J. P. M.; Stone, A. J.; Taylor, R.; Allen, F. H. The nature and geometry of intermolecular interactions between halogens and oxygen or nitrogen. *J. Am. Chem. Soc.* **1996**, *118*, 3108−3116.
(41) Du, F.; Wang, H.; Zhang, Z.; Yang, L.; Cao, J.; Yu, J.; Tang, W. An unfused-ring acceptor with high side-chain economy enabling 11.17% as-cast organic solar cells. *Mater. Horiz.* **2021**, *8*, 1008−1016.
(42) Xu, C.; Ma, X.; Zhao, Z.; Jiang, M.; Hu, Z.; Gao, J.; Deng, Z.; Zhou, Z.; An, Q.; Zhang, J.; Zhang, F. Over 17.6% Efficiency organic photovoltaic devices with two compatible polymer donors. *Sol. RRL* **2021**, *5*, No. 2100175.